Journal of Ocean and Wind Energy (ISSN 2310-3604)
Copyright © by The International Society of Offshore and Polar Engineers
Vol. 2, No. 2, May 2015, pp. 98–106; http://dx.doi.org/10.17736/jowe.2015.ilr03

http://www.isope.org/publications/publications.htm

Quantification of Wave Model Uncertainties Used for Probabilistic Reliability Assessments of Wave Energy Converters

Simon Ambühl*, Jens Peter Kofoed and John D. Sørensen
Department of Civil Engineering, Aalborg University
Aalborg, Denmark

Wave models used for site assessments are subjected to model uncertainties, which need to be quantified when using wave model results for probabilistic reliability assessments. This paper focuses on determination of wave model uncertainties. Four different wave models are considered, and validation data are collected from published scientific research. The bias and the root-mean-square error, as well as the scatter index, are considered for the significant wave height as well as the mean zero-crossing wave period. Based on an illustrative generic example, this paper presents how the quantified uncertainties can be implemented in probabilistic reliability assessments.

INTRODUCTION

Before wave energy converters (WECs) can be installed, a site assessment needs to be performed in order to characterize the environmental conditions for a particular location for WECs. The site assessment should ascertain the spatial and temporal variation of the wave resources (metocean environment), including their uncertainties as well as the bathymetry of the location. The site assessment makes it possible to find the cost-optimized location for the device. In this context, cost optimization means maximizing the benefit. The benefit is influenced by the environmental conditions as well as the location itself. The environmental conditions define the production rate of electricity but also the loads onto the structure, and the location influences the accessibility of the device as well as the cost of the mooring system. Furthermore, potential interference between multiple converters should be identified by the site assessment.

Measurement data from buoys will provide only point measurements, whereas simulated data enable coverage of the whole area of a potentially exploitable site for WECs. Furthermore, obtaining measured wave data from buoys is time-consuming and costly. Therefore, so-called wave models (e.g., SWAN, WAM, WAVEWATCH III, and MIKE21 SW) are often used to simulate wave conditions in a certain domain and are popular for site assessments of potential wave energy device locations (EquiMar, 2010).

The simulated results from wave models need to be validated by using measured wave data from a point within the considered domain in order to assess their accuracy. The output from wave models often contains significant wave height and wave period (peak or mean zero-crossing wave period) data. Significant wave height, H_S, and peak wave period, T_P, distributions are often taken to assess site-specific extreme and fatigue wave loads onto a certain WEC structure based on, e.g., wave elevation time series of a certain wave state given by H_S and T_P. From the structural design of the device, the structural reliability can be estimated.

When probabilistic reliability assessments are used, the uncertainties related to data sets from wave models need to be quantified. The purpose of this paper is to quantify the uncertainties related to wave models based on published validation results. These uncertainties can be used for wave simulations where no validation is available. Furthermore, uncertainties should be determined when structural reliability assessments of WECs are performed and the environmental data are simulated by different wave models.

This paper first gives a short introduction of the wave models used, how their accuracy is defined, and the potential uncertainty sources of wave models as well as a short introduction of probabilistic reliability assessments. In the next section, validation data from published work and publicly available validation data are compared, and uncertainties related to wave models are estimated. Furthermore, a generic illustrative example using the Wavestar WEC shows how the wave model uncertainties can be implemented in probabilistic reliability assessments.

BACKGROUND INFORMATION

Definition of Wave States

Wave states are often defined using the significant wave height H_S and peak period T_P or the mean zero-crossing wave period T_Z. The significant wave height describes (in the time domain) the mean wave height of the highest third of the waves. The mean zero-crossing wave period is the mean value of all considered waves. The peak period, which can be extracted from the spectrum, indicates the wave period with its highest energy. These values might be measured by a buoy and can be assumed to describe wave conditions with considered time frames between 20 minutes and 6 hours, where the wave state can be assumed to be stationary (DNV, 2010).

For load calculations (extreme and fatigue), time series of wave elevations from the wave state parameters H_S, T_P/T_Z can be derived by using a certain spectrum. For North Sea applications, the JONSWAP spectrum can be taken. Uncertainties related to the spectrum given a certain wave state, as well as the statistical uncertainty based on different considered time series lengths for H_S and T_P/T_Z estimations, are not considered here. Information about statistical uncertainties related to wave states can be found in Ambühl et al. (2013).

*ISOPE Member.

Received August 12, 2014; updated and further revised manuscript received by the editors November 6, 2014. The original version (prior to the final updated and revised manuscript) was presented at the Twenty-fourth International Ocean and Polar Engineering Conference (ISOPE-2014), Busan, Korea, June 15–20, 2014.
KEY WORDS: Reliability, uncertainty, wave models, wave energy converters, wave conditions, Wavestar.

Simulation Tools for Wave State Simulations

Currently, potential wave energy device locations are often in shallow water and nearshore in order to have high accessibility and low mooring costs. Wave models can be used to transform data from well-described deepsea regions to shallow-water regions. These models take into account the local bathymetry and the coastal topography as well as wind and current data. When the considered area for simulation only includes nearshore locations, the wave state data from a buoy can be used as an input parameter.

There are different simulation tools available for simulating wave states at a specific location. Currently, the industry and the scientific community use the third generation of wave models, which describe all wave evolution processes based on physical background, instead of arbitrary models. Popular spectral wave models used by the industry and in research are SWAN (SWAN Team, 2013), WAVEWATCH III (Tolman, 2009), MIKE21 SW (DHI, 2013), and WAM (WAMDI Group, 1988). The spectral wave models model processes like wind-generated waves, nonlinear interactions, white-capping (dissipation of energy due to breaking of waves in deeper sea), bottom friction, shallow-water depth-induced breaking, advection (reflecting the transport of, e.g., heat and salinity), refraction, and shoaling in coastal areas.

Most simulation tools make it possible to use irregular and unstructured grid sizes where the grid can be refined in coastal areas. The geographical simulation domain can cover, e.g., the North Atlantic or the North Sea, but wave models can also be used to estimate wave characteristics in smaller ranges like nearshore regions (coastal areas). The wave models can be used for hindcast simulations where, e.g., buoy measurement data are used for the input data at the open sea boundary. This hindcast simulation can then be used to characterize the wave characteristics at locations within the simulation domain. However, wave characteristic forecast simulations for several hours to several days also can be performed with these wave models.

Sources of Uncertainties of Wave Models

Figure 1 shows different sources of uncertainties of wave model simulation and how they propagate when wave models are used to simulate wave conditions.

The buoy data, which are used as input data for hindcast wave state simulations or validation of simulation results, might lack certain time durations. The moored buoy can move around the anchoring point, and movements of the buoy may lead to location uncertainties when fine grids are used. Furthermore, buoys often underestimate extreme wave heights of steep waves because they are going through or along the crest. Deepwater buoy measurements and wind measurements show conditions for a certain point, whereas for wave state simulations, these measurements are often applied along the offshore boundary and introduce some location/modeling uncertainties. Sometimes the input data used for the wave models are already simulated data (e.g., simulation of tidal movements at a certain location) and, therefore, the model uncertainties from the prior simulation are propagating in the wave model. Furthermore, current, tides, wave, and wind data contain measurement uncertainties of the measurement devices. The accuracy of bathymetry data becomes important for nearshore applications. Its accuracy depends on the grid size of the data as well as the way it is determined. In this paper, data are collected from published validation results performed by others. The validation data are taken from the different sources shown in Table 7.

Spectral wave models contain different submodels that model certain physical phenomena. The growth of water waves by wind as well as wave interactions are based on models and simplifications concerning, e.g., nonlinear effects. Furthermore, dissipation of energy due to breaking waves and bottom friction needs to be modeled. Also, wave propagation is modeled in a way accounting for effects like shoaling, refraction, diffraction, and reflection. Further information about uncertainties related to wave models can be found in Cavaleri et al. (2007).

Numerical uncertainties due to truncation errors occur when an infinite sum is approximated using a finite sum. This occurs when numerical integration is needed or Fourier transform is performed. Uncertainties related to the simulation resolution depend on the grid size as well as the time. Smaller grids and smaller time steps lead to smaller resolution uncertainties, but they increase the simulation costs.

In general, there are aleatory and epistemic uncertainties for each wave model. Epistemic uncertainties are related to model uncertainties, limited amounts of data (statistical uncertainty), and measurement uncertainties. These uncertainties can be decreased by increasing the complexity of the simulation. However, aleatory (physical) uncertainties that are related to the randomness of nature cannot be decreased and also remain in an accurate simulation. In this case, an aleatory uncertainty could be interannual variation of extreme values. When considering the published validation data, as performed in this paper, only the resulting wave model uncertainty can be quantified, not the uncertainties of the different steps shown in Fig. 1.

Quantification of Uncertainties

In order to validate results from wave state simulations, the (hindcast) simulation results are compared with measured wave states from a buoy at a certain location and the same time period. For quantification of uncertainties, statistical measures like bias (B) and root-mean-square error ($RMSE$), as well as the scatter index (SI), are calculated for a certain buoy measurement data set (see, e.g., EquiMar, 2010):

$$B = \frac{1}{n}\sum_{i=1}^{n}(o-m)_i \tag{1}$$

$$RMSE = \sqrt{\frac{1}{n}\sum_{i=1}^{n}(o-m)_i^2} \tag{2}$$

$$SI = \frac{RMSE}{\overline{o}} \tag{3}$$

where n is the number of data points, m_i is the model-derived wave parameter at data point i, and o_i is the corresponding measured wave data. The mean value of the observed data ($\overline{o}$) is also considered in the formula above. The bias B gives information on whether the model generally over- or underestimates the simulated parameter. The root-mean-square error $RMSE$ indicates the differences between the observed and modeled values (residuals). The scatter index SI puts the $RMSE$ in a relative frame. An ideal model, which reflects nature perfectly, shows bias B and the root-mean-square error $RMSE$, as well as the scatter index SI, equal to 0.

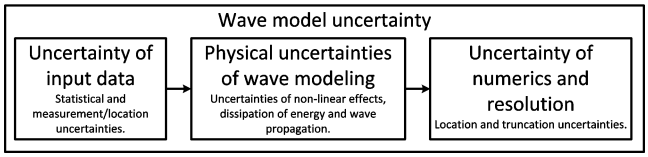

Fig. 1 Different sources of uncertainties to be considered in wave model simulations

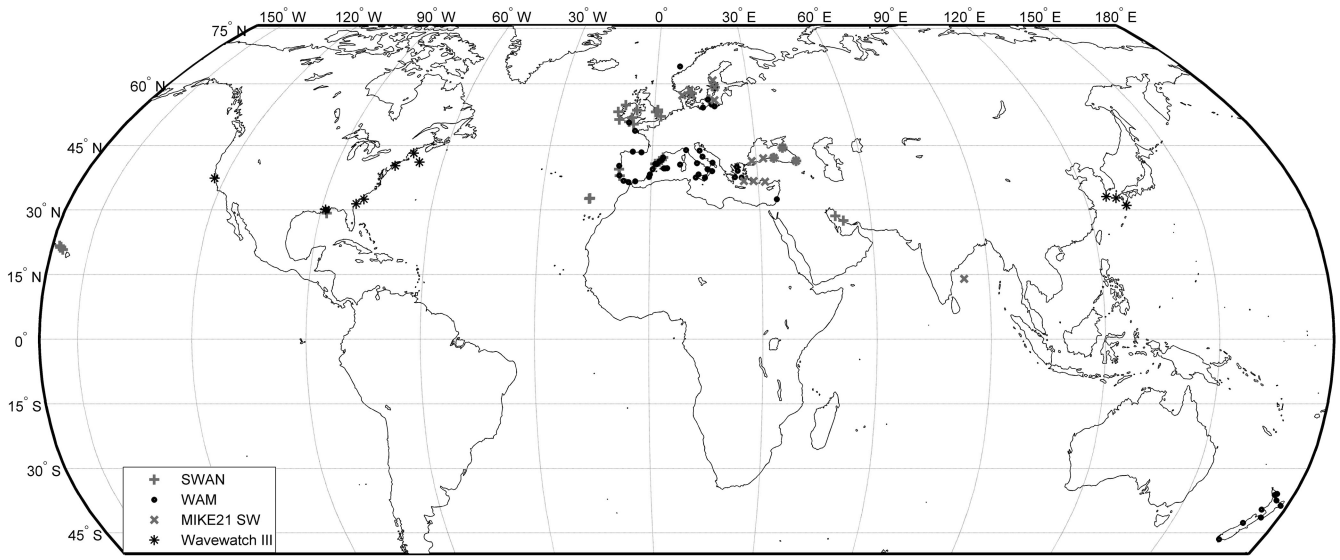

Fig. 2 Locations where buoy measurements are available for wave model calibrations for different wave models. More information about the locations can be found in Table 7

When a data set of B, $RMSE$, and SI values are available, statistics resulting in a certain mean value and a standard deviation can be determined:

$$\overline{X} = \mu_X = \frac{1}{N}\sum_{j=1}^{N} X_j$$
$$\sigma_X = \sqrt{\frac{1}{N-1}\sum_{j=1}^{N}(X_j - \overline{X})^2} \tag{4}$$

where $\overline{X}$ is the mean value, σ_X is the standard deviation of the parameter $X = [B, SI, RMSE]$, and N indicates the number of considered validation results. Statistics can be performed for validation results within a certain water depth range or for a certain wave model.

Another way to estimate model uncertainties is explained in EN 1990 (2002), Appendix D, where the approach is explained for test results to estimate material properties. This approach can be transferred and also applied to simulation results.

Probabilistic Reliability Assessments

Probabilistic reliability assessments consider uncertainties related, e.g., to the environmental conditions or the load calculation method. This approach can be used to estimate the probability of failure of a certain structural component and a certain failure mode. The uncertain parameters are modeled by stochastic variables or processes/fields. In probabilistic reliability assessments, aleatory as well as epistemic uncertainties can be considered.

The failure mode is assumed to be modeled by a limit state equation $g(\mathbf{X})$ where the stochastic variables $\mathbf{X}$ are included. The limit state equation represents the limit state of a certain structural failure mode like sliding, overturning, buckling, or fatigue failure. The probability of failure, P_F, described by a failure mode can be calculated by using the FORM/SORM approach, where the most probable failure point is calculated, or simulation techniques. The reliability index β can be determined by:

$$P_F = P_F\left(g(\mathbf{X}) \le 0\right) \approx \Phi(-\beta) \tag{5}$$

where $\Phi(\ )$ is the standard normal distribution function. For more information about probabilistic reliability analyses using structural reliability methods, see, e.g., Lemaire et al. (2009) or Madsen et al. (1986).

DETERMINATION OF WAVE MODEL UNCERTAINTIES

In this paper the uncertainties of wave models represented by the bias B, the root-mean-square error $RMSE$, and the scatter index SI are quantified. These values are estimated for the significant wave height and the mean zero-crossing wave period. Wave model simulations should be validated with, e.g., buoy measurements from a location within the simulated domain. Here different buoy validation results of different wave models are collected from published articles (see Table 7). Water depths up to 300 m are considered here. Figure 2 shows the considered locations where buoy measurements for wave model validations are available. The considered validation sets need to have a minimal duration of one year in order to cover all wave characteristics (like winter storms) of a certain location.

Table 1 shows the estimated mean bias ($\overline{B}$), the mean $RMSE$ value ($\overline{RMSE}$), and the mean scatter index ($\overline{SI}$) for the significant wave height and different wave models. The data in Table 1 are based on collected validation results published in articles by others, and Table 7 gives an overview of these published articles. From these articles, validation results (B, $RMSE$, and SI) of the significant wave height and the mean zero-crossing wave period are taken for a certain location (water depth) and a certain wave model. The values $\overline{B}$, $\overline{RMSE}$, and $\overline{SI}$ in Table 1 for a certain wave

Meaning	SWAN	WAM	MIKE21	WW III
$\overline{B}_{H_S}$ (m)	0.0713	0.1085	0.0113	−0.0190
$\overline{RMSE}_{H_S}$ (m)	0.4436	0.4665	0.3000	0.3760
$\overline{SI}_{H_S}$(–)	0.3316	0.3763	0.3644	0.2396

Table 1 Uncertainty about H_S simulation results from different wave models considering all available data. $\overline{B}_{H_S}$ shows mean bias value; $\overline{RMSE}_{H_S}$ shows mean $RMSE$; $\overline{SI}_{H_S}$ is equal to the mean scatter index value of H_S.

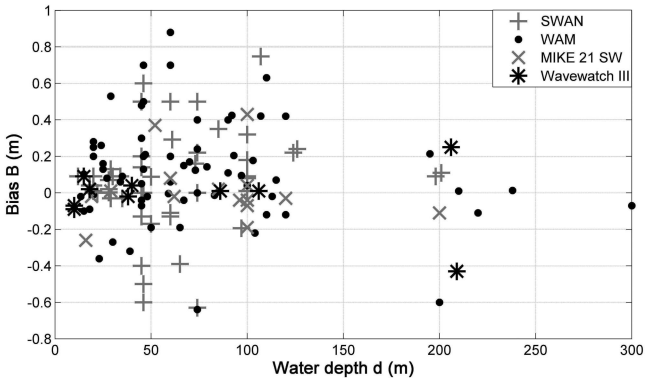

Fig. 3 Bias B values of significant wave height (H_S) for different water depths and different wave models

model represent the mean values of the values taken from the published articles shown in Table 7.

The wave models SWAN, WAM, and MIKE21 SW show a slight underestimation of the significant wave height compared with buoy data, whereas the WAVEWATCH III shows a small overestimation of the significant wave height. Values for $\overline{RMSE}$ are in the range between 0.3 m and 0.47 m. The smallest mean *RMSE* values show for MIKE21 SW simulations and the largest values for WAM simulation data. The mean scatter index *SI* for the significant wave height is between 0.24 and 0.38.

It is assumed that the bathymetry impacts the accuracy of the modeled wave data. The bathymetry is reflected here with different water depths. Figure 3 shows the bias B resulting from different wave models dependent on the water depth. The bias is less scattered for all different wave models when the water depth increases, whereas its mean values remain roughly constant when the water depth is changed.

The tendency for *RMSE* to be dependent on the water depth is shown in Fig. 4. For SWAN, WAM, and WAVEWATCH III, the *RMSE* value decreases when the water depth is increased, whereas for MIKE21 SW, the *RMSE* value increases when the water depth is increased.

Figure 5 shows the scatter index *SI* for buoy measurement validations at different water depths and different wave models. The scatter index slightly decreases for SWAN and MIKE21 SW simulations. The WAM model results in a more or less constant significant wave height scatter index for different water depths, whereas for WAVEWATCH III simulations, the scatter index increases slightly for increased water depths.

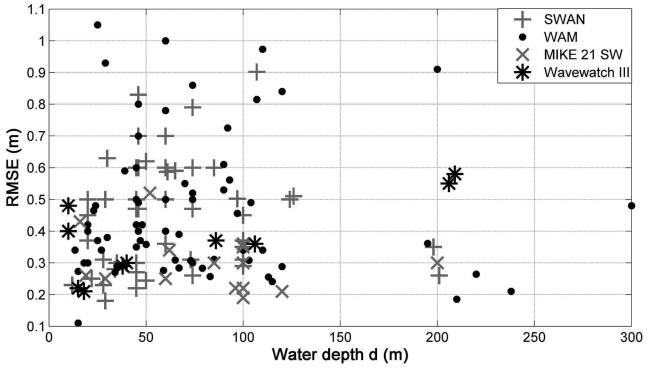

Fig. 4 Root-mean-square *RMSE* values of significant wave height (H_S) for different water depths and different wave models

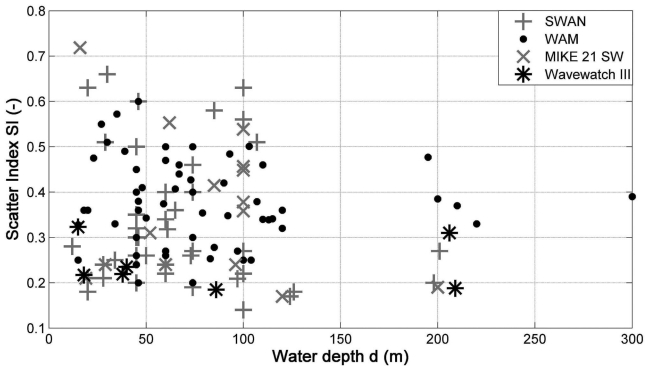

Fig. 5 Scatter index *SI* values of significant wave height (H_S) for different water depths and different wave models

Meaning	SWAN	WAM	MIKE21	WW III*
$\overline{B}_{T_Z}$ (s)	0.2034	−0.1800	0.0321	—
$\overline{RMSE}_{T_Z}$ (s)	2.5673	1.1789	0.7986	—
$\overline{SI}_{T_Z}$ (−)	0.3640	0.2303	0.1830	—

* WW III: WAVEWATCH III

Table 2 Uncertainty about T_Z simulation results from different wave models considering all available data

For the mean zero-crossing wave period T_Z, also bias B, root-mean-square error *RMSE* and scatter index *SI* data are available (taken from references shown in Table 7). For WAVEWATCH III simulations, no T_Z data are available. Table 2 shows the mean values of bias B and root-mean-square error *RMSE* as well as the mean scatter index *SI* of the modeled mean zero-crossing wave period for different wave models. The SWAN model tends to underestimate the mean zero-crossing wave period, whereas the WAM model shows a slightly overestimated mean zero-crossing wave period, and the MIKE21 SW wave model indicates no significant bias value. The largest scattering occurs for the SWAN simulations. The smallest scattering is observed for the MIKE21 SW model.

The uncertainty values, like bias B, root-mean-square error *RMSE*, or scatter index *SI*, of the mean zero-crossing wave period are dependent on the water depth. Figure 6 shows the considered bias values of the mean zero-crossing wave period dependent on the water depth. The bias value increases for SWAN simulations, whereas for the two other wave models, the bias remains more or less independent of the water depth. Figure 7 shows the root-

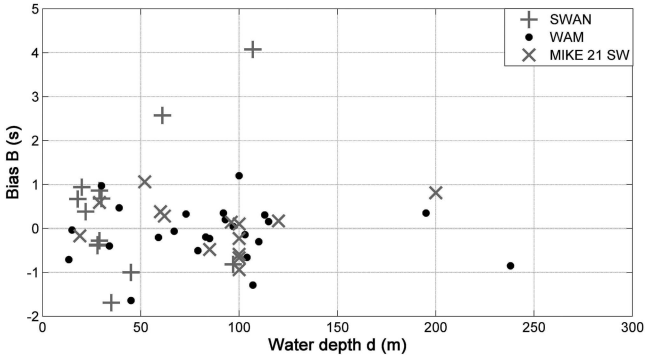

Fig. 6 Bias values of mean zero-crossing wave period (T_Z) for different water depths and different wave models

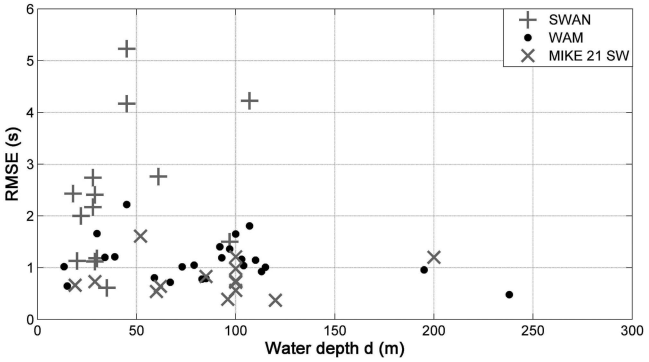

Fig. 7 *RMSE* values of mean zero-crossing wave period (T_Z) for different water depths and different wave models

mean-square error *RMSE* for the three wave models dependent on the water depth. The *RMSE* values increase for SWAN models when moving to larger water depths, whereas the MIKE21 SW, as well as the WAM, model leads to *RMSE* values that are not strongly dependent on the water depth. Figure 8 shows the scatter index *SI* of T_Z dependent on the water depth. Here the considered validation results from SWAN models also show increased scattering when the water depth is increased, whereas the two other wave models lead to scatter indices more or less independent of the water depth.

In order to give a general statement about the uncertainties of the bias *B*, the root-mean-square error *RMSE* values, and the scatter index *SI* of the significant wave height and the mean zero-crossing wave period, all data from the different wave models are considered and arranged in water depth sections. Furthermore, Figs. 3 to 8 indicate that the considered variables (*B*, *RMSE*, *SI*) are uncertain themselves and should be modeled by a stochastic variable. Table 3 shows statistical information about the bias *B* and root-mean-square error *RMSE*, as well as scatter index *SI* values of H_S presented in Figs. 3 to 5 for different water depth ranges, including data from all wave models. Water depths up to 150 m are considered because, for larger water depths, the number of available values is too low.

The simulated significant wave height is, in general, underestimated compared with the measured data. The bias of the significant wave height reaches the smallest values for water depths below 50 m. For larger water depth ranges, the mean bias value is increased by roughly 0.055 m at every 50 m water depth increase. Also, the scattering of the significant wave height increases when the water depth increases. The mean scatter index of the significant wave height is equal to 0.27 for water depths less than

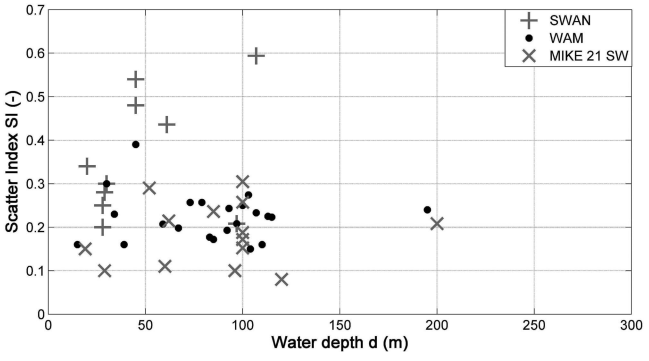

Fig. 8 Scatter index values of mean zero-crossing wave period (T_Z) for different water depths and different wave models

Water depth d (m)		< 50	50–100	100–150
No. of considered data sets		65	52	14
B_{H_S} (m)	$\mu_{B_{H_S}}$	0.06	0.12	0.17
	$\sigma_{B_{H_S}}$	0.24	0.30	0.29
$RMSE_{H_S}$ (m)	$\mu_{RMSE_{H_S}}$	0.42	0.48	0.50
	$\sigma_{RMSE_{H_S}}$	0.19	0.19	0.27
SI_{H_S} (−)	$\mu_{SI_{H_S}}$	0.27	0.31	0.33
	$\sigma_{SI_{H_S}}$	0.20	0.13	0.14

Table 3 Significant wave height uncertainty of bias B_{H_S}, root-mean-square error $RMSE_{H_S}$, and scatter index SI_{H_S} for three different water depth ranges considering all results from the different wave models presented in Figs. 3 to 5

Water depth (m)		< 50	50–100	100–150
No. of considered data sets		22	16	8
B_{T_Z} (s)	$\mu_{B_{T_Z}}$	−0.23	0.18	0.29
	$\sigma_{B_{T_Z}}$	0.86	0.78	1.62
$RMSE_{T_Z}$ (s)	$\mu_{RMSE_{T_Z}}$	2.01	1.09	1.46
	$\sigma_{RMSE_{T_Z}}$	1.35	0.57	1.18
SI_{T_Z} (–)	$\mu_{SI_{T_Z}}$	0.23	0.22	0.24
	$\sigma_{SI_{T_Z}}$	0.17	0.08	0.15

Table 4 Mean zero-crossing wave period uncertainty of bias B_{T_Z}, root-mean-square error $RMSE_{T_Z}$, and scatter index SI_{T_Z} for three different water depth ranges considering all results from the different wave models presented in Figs. 6 to 8

50 m, and its value increases to 0.33 when reaching water depths between 100 and 150 m.

Table 4 shows the statistical information for the zero-crossing wave period. The considered data in Table 4 contain the data presented in Figs. 6 to 8 for different water depth ranges, including all different wave models. The mean zero-crossing wave period bias increases when the water depth increases. For water depths less than 50 m, the simulated mean zero-crossing wave period is slightly overestimated, whereas it is underestimated for water depths larger than 50 m. The mean scatter index of the zero-crossing wave period is constant for different water depths. The highest accuracy of the considered data and wave models occurs for water depths between 50 and 100 m. In this range, the bias, the root-mean-square error, and the scatter index have the smallest values.

GENERIC EXAMPLE

The following generic example shows how wave model uncertainties can be implemented in probabilistic reliability assessments. This section considers a simple limit state that focuses on the bending of the Wavestar piles due to extreme slamming loads of breaking waves. Figure 9 shows a photograph of the Wavestar prototype located at the Danish North Sea coast near Hanstholm, Denmark. The device consists of four piles, two floaters, and a main platform that carries different electrical and mechanical components. Electricity is produced by a hydraulic cycle that transfers the kinetic energy of the floaters to a turbine. The turbine then impels a generator. The floaters of the device can be moved up from the water surface into so-called “storm protection

Fig. 9 Photo of Wavestar prototype with one floater on water surface ("production mode") and one lifted from water surface ("storm protection mode")

mode" (see Fig. 9) in order to limit extreme wave loads onto the floater structure.

The generic example is based on a static approach and only considers extreme slamming wave loads, which are assumed to be the dominating load during storm conditions. Wind loads, as well as current loads, are not considered in this generic example.

The piles are thin-walled hollow structures. The limit state equation of the failure mode "Bending failure of piles due to slamming of breaking wave loads" can be written as:

$$g = M_{cr} - l \cdot F_S \cdot X_S \cdot X_{\text{dyn}} \tag{6}$$

where M_{cr} is the critical bending capacity, F_S is the horizontal slamming force due to breaking extreme waves, X_S indicates the uncertainties related with slamming load assessments, and X_{dyn} represents the uncertainty of using a static 2D approach compared with a dynamic behavior that includes the global structure of the device and soil properties. The variable l indicates the mean height at which the waves are slamming into the pile. The critical bending moment can be calculated according to:

$$M_{cr} = \frac{1}{6}\left(1 - 0.84\frac{D}{t}\frac{F_y X_{F_y}}{E X_E}\right)\left[D^3 - (D-2t)^3\right] F_y X_{F_y} X_{cr} \tag{7}$$

where D is the diameter of the pile, t is the thickness of the pile, F_y is the yield stress of structural steel (including material uncertainties), X_{F_y} is the model uncertainty related to yield stress, E is the Young's modulus of structural steel (including material uncertainties), X_E is its model uncertainty, and X_{cr} is the model uncertainty of critical load capacity (see Tarp-Johansen et al., 2002). Table 5 shows information about the values and distribution parameters used for the reliability assessment. Values for the pile diameter D, as well as the thickness t, are taken from the prototype at Hanstholm. The pile diameter is equal to 2 m and the thickness of the pile is 5 cm.

The extreme slamming wave loads, F_S, consider slamming loads of a wave breaking in front of the pile. The highest horizontal peak wave load while the breaking wave is passing the cylinder cross-section can be calculated according to Goda et al. (1966):

$$F_S = \frac{\pi \rho_w D C_b^2 N_b \lambda}{2} \tag{8}$$

where ρ_w is the water density, N_b is the maximum surface elevation when the wave is breaking, λ is the curling factor, and C_b is the wave celerity. It is assumed in Eq. 8 that the vertical breaker front has height equal to λN_b and moves with celerity C_b. The maximum surface wave elevation N_b at breaking can be calculated according to:

$$N_b = \mu C H_{s,\text{annual}} \tag{9}$$

where μ is the horizontal asymmetry considering the amount of the wave height above the mean seawater level. This value is esti-

Variable	Meaning	Dist. type	Expected value	Std. dev.	Source
$H_{S,\text{annual},wm}$	Annual ext. H_S wave model	G	5.27 m	0.56 m	DHI (2013b)
C	Factor for inst. wave height	G	1.86	0.17	Ambühl et al. (2013)
B_{H_S}	Bias unc. H_S	N	0.06 m	0.24 m	Table 3
$RMSE_{H_S}$	*RMSE* H_S	N	0.42 m	0.19 m	Table 3
$T_Z(H_{S,\text{annual},wm})$	Unc. of T_Z given $H_{S,\text{annual},wm}$	LN	8.54 s	1.02 s	DHI (2013b)
B_{T_Z}	Bias unc. T_Z	N	−0.23 s	0.86 s	Table 4
$RMSE_{T_Z}$	*RMSE* T_Z	N	2.01 s	1.35 s	Table 4
d	Water depth	D	17 m		DHI (2013b)
D	Diameter pile	D	2 m		Prototype
t	Thickness pile	D	0.05 m		Prototype
g	Accel. of gravity	D	9.81 m/s^2		
ρ_w	H_20 density	D	1000 kg/m^3		
E	Young's modulus	LN	2.1 10^5 MPa	4200 MPa	Tarp-Johansen et al. (2002)
X_E	Unc. Young's modulus	LN	1	0.02	Tarp-Johansen et al. (2002)
F_y	Yield stress	LN	240 MPa	12 MPa	Tarp-Johansen et al. (2002)
X_{F_y}	Unc. yield stress	LN	1	0.05	Tarp-Johansen et al. (2002)
X_{cr}	Unc. bending model	LN	1	0.05	JCSS (2001)
X_{dyn}	Unc. dynamic response	LN	1	0.1	JCSS (2001)
X_S	Unc. slamming loads	LN	1	0, 0.1, 0.2, 0.3	
λ	Curling factor	D	0.4		Goda et al. (1966)
μ	Horizontal asymmetry factor	N	0.6	0.1	Myrhaug and Kjeldsen (1986)

Dist.: distribution; std. dev.: standard deviation; ext.: extreme; inst.: instantaneous; unc.: uncertainty; accel.: acceleration; D: deterministic; G: Gumbel; LN: log normal; N: normal.

Table 5 Stochastic model used for failure mode "Bending failure of pile due to extreme slamming wave loads"

mated based on measurements in Myrhaug and Kjeldsen (1986). $H_{S,\text{annual}}$ gives the annual extreme significant wave height, and C is the factor leading from the significant wave height to the extreme instantaneous wave height during three hours of wave elevation at a certain wave state.

The wave celerity C_b using linear wave theory is equal to:

$$C_b = \frac{gT(H_{S,\text{annual}})}{2\pi} \tanh\left(\frac{2\pi d}{L}\right) \tag{10}$$

where $T(H_{S,\text{annual}})$ is the wave period given $H_{S,\text{annual}}$, d is the water depth, and L is the wave length.

The length l (see Eq. 6) in this case is assumed to be equal to:

$$l = d + (1 - \lambda/2)\, N_b \tag{11}$$

The annual extreme significant wave height $H_{S,\text{annual}}$ can be calculated from the sum of the annual extreme significant wave height estimated from the wave model ($H_{S,\text{annual},wm}$) and the uncertainty related to wave model, B_{H_S}, which is assumed to be a normal distributed variable ($N(B_{H_S}, RMS_{H_S})$) with mean value equal to the bias of H_S and the standard deviation equal to the root-mean-square error of H_S. Because the bias value and the root-mean-square error are uncertain (see Figs. 3 and 4), these values are modeled as stochastic variables. The resulting annual extreme significant wave height, $H_{S,\text{annual}}$, can be calculated in the following way:

$$H_{S,\text{annual}} = H_{S,\text{annual},wm} + B_{H_s} \tag{12}$$

The same approach can be used for calculating the mean zero-crossing wave period $T_Z(H_{S,\text{annual}})$:

$$T_Z = T_Z\left(H_{S,\text{annual},wm}\right) + B_{T_Z} \tag{13}$$

where B_{T_Z} is normal distributed with mean value B_{T_Z} and standard deviation $RMSE_{T_Z}$ $\left(B_{T_Z} = N\left(B_{T_Z}, RMSE_{T_Z}\right)\right)$. It represents the normal distributed uncertainty about the mean zero-crossing wave period from the wave models. Also, for the mean zero-crossing wave period, the bias, B_{T_Z}, and the root-mean-square error, $RMSE_{T_Z}$, are related to uncertainties and modeled as stochastic variables.

The annual extreme significant wave height, as well as the mean wave period conditional on the significant wave height, is calculated based on a hindcast simulation over 31 years using MIKE21 SW. The uncertainties of the numerics (truncation errors) are assumed to be negligible.

The reliability assessment will use Comrel software (see RCP GmbH, 2004) and the stochastic model shown in Table 5. Table 6 shows the annual reliability index and the corresponding annual probability of failure for different slamming load uncertainties (X_S) with and without considering the wave model uncertainties of H_S and T_Z. For this generic example, the consideration of wave modeling uncertainties increases the probability of failure compared with no consideration. Furthermore, it increases the probability of failure when the uncertainty is increased related to the modeling of slamming loads. Annual minimal reliability indices of structural components for offshore wind turbines are accepted to be in the range between 3.1 and 3.7. The resulting annual reliability index for this generic failure mode is within this range when the slamming load is smaller than 0.2.

	With wave model unc.		Without wave model unc.	
Std. dev. X_S	β	P_F	β	P_F
0.0	3.38	$3.59\ 10^{-4}$	3.59	$1.89\ 10^{-4}$
0.1	3.27	$5.54\ 10^{-4}$	3.44	$2.89\ 10^{-4}$
0.2	2.97	$1.47\ 10^{-3}$	3.13	$8.70\ 10^{-4}$
0.3	2.63	$4.22\ 10^{-3}$	2.76	$2.88\ 10^{-3}$

Std. dev: standard deviation; unc.: uncertainty.

Table 6 Resulting annual reliability index (β) and the corresponding annual probability of failure (P_F) due to slamming loads at the piles including wave model uncertainty and without wave model uncertainty ($H_{S,\text{annual}} = H_{S,\text{annual},wm}$ and $T_Z = T_Z(H_{S,\text{annual},wm})$)

CONCLUSIONS

Validation results of wave models using buoy measurement data are collected in this paper in order to assess the uncertainty related to wave models, which are often used for site assessments of WECs. Uncertainties related to the bias and the root-mean-square error, as well as the scatter index, are collected from published validation data for the significant wave height and the mean zero-crossing wave period. The resulting uncertainties can be used and included in probabilistic structural reliability assessments of WECs. An illustrative generic example focusing on the bending failure of the Wavestar device piles due to extreme wave slamming loads shows how the uncertainties can be implemented in probabilistic reliability assessments.

ACKNOWLEDGEMENTS

The authors gratefully acknowledge the financial support of the Danish Council for Strategic Research under the Programme Commission on Sustainable Energy and Environment (Contract 09-67257, Structural Design of Wave Energy Devices), which made this work possible.

REFERENCES

Akpınar, A, van Vledder, G, Kömürcü, MI, and Özger, M (2012). "Evaluation of the Numerical Wave Model (SWAN) for Wave Simulation in the Black Sea," *Cont Shelf Res*, 50–51, 80–99. http://dx.doi.org/10.1016/j.csr.2012.09.012.

Ambühl, S, Kofoed, JP, and Sørensen, JD (2013). "Influence of Wave State Uncertainties on Probabilistic Assessments of Wave Energy Devices," *Proc 10th Eur Wave Tidal Conf*, Aalborg, Denmark, EWTEC, 11 pp.

Ayat, B (2013). "Wave Power Atlas of Eastern Mediterranean and Aegean Seas," *Energy*, 54, 251–262. http://dx.doi.org/10.1016/j.energy.2013.02.060.

Aydoğan, B, Ayat, B, and Yüksel, Y (2013). "Black Sea Wave Energy Atlas from 13 Years Hindcasted Wave Data," *Renewable Energy*, 57, 436–447. http://dx.doi.org/10.1016/j.renene.2013.01.047.

Bento, AR, Martinho, P, and Soares, CG (2011). "Modelling Wave Energy Resources for UK's Southwest Coast," *Proc OCEANS 2011*, Santander, Spain, IEEE, 1–8. http://dx.doi.org/10.1109/Oceans-Spain.2011.6003533.

Berg, C (2008). "Validation of the WAM Model over the Baltic Sea," In: *Examensarbete vid Institutionen för geovetenskaper*, ISSN 1650-6553, Nr 156, Uppsala, Sweden.

Bolaños-Sanchez, B, Sanchez-Arcilla, A, and Cateura, J (2007). "Evaluation of Two Atmospheric Models for Wind–Wave Modelling in the NW Mediterranean," *J Mar Syst*, 65(1–4), 336–353. http://dx.doi.org/10.1016/j.jmarsys.2005.09.014.

Carretero Albiach, JC, Alvarez Fanjul, E, Gómez Lahoz, M, Perez Gomez, B, and Rodrıguez Sanchez-Arevalo, I (2000). "Ocean Forecasting in Narrow Shelf Seas: Application to the Spanish Coasts," *Coastal Eng*, 41(1–3), 269–293. http://dx.doi.org/10.1016/S0378-3839(00)00035-1.

Cavaleri, L, et al. (2007). "Wave Modelling: The State of the Art," *Prog Oceanogr*, 75(4), 603–674. http://dx.doi.org/10.1016/j.pocean.2007.05.005.

Chawla, A, Spindler, DM, and Tolman, HL (2013). "Validation of a Thirty Year Wave Hindcast Using the Climate Forecast System Reanalysis Winds," *Ocean Model*, 70, 189–206. http://dx.doi.org/10.1016/j.ocemod.2012.07.005.

Cieślikiewicz, W, and Paplińska-Swerpel, B (2008). "A 44-Year Hindcast of Wind Wave Fields over the Baltic Sea," *Coastal Eng*, 55(11), 894–905. http://dx.doi.org/10.1016/j.coastaleng.2008.02.017.

DHI (2013a). *MIKE 21 Wave Modelling: Short Description*, Danish Hydraulic Institute (DHI), Hørsholm, Denmark.

DHI (2013b). *Structural Design of Wave Energy Devices: Long-Term Wave Prediction*, Deliverable D1.1, Danish Hydraulic Institute (DHI), Hørsholm, Denmark.

DNV (2010). *Environmental Conditions and Environmental Loads*, Recommended Practice DNV-RP-C205, Det Norske Veritas, Høvik, Norway.

Dykes, JD, Hsu, YL, and Rogers, WE (2002). "The Development of an Operational SWAN Model for NGLI," *Proc OCEANS 2002*, Hattiesburg, MS, USA, MTS/IEEE, 2, 859–866. http://dx.doi.org/10.1109/OCEANS.2002.1192081.

EquiMar (2010). *Deliverable D2.3: Application of Numerical Models*, Equitable Testing and Evaluation of Marine Energy Extraction Devices in terms of Performance, Cost and Environmental Impact.

EN 1990 (2002). *Eurocode: Basis of Structural Design*, European Standard, European Committee for Standardization, Brussels, Belgium.

Goda, Y, Haranaka, S, and Kitahata, M (1966). *Study of Impulsive Breaking Wave Forces on Piles*, Port and Harbor Research Institute Report, 5(6), 1–30 (in Japanese).

Gorman, RM, Bryan, KR, and Laing, AK (2003). "Wave Hindcast for the New Zealand Region: Nearshore Validation and Coastal Wave Climate," *N Z J Mar Freshwater Res*, 37(3), 567–588. http://dx.doi.org/10.1080/00288330.2003.9517190.

Holmbom, K (2011). *Modelling of Waves and Currents in the Baltic Sea*, TRITA LWR Degree Project 11:04, ISSN 1651-064X.

JCSS (2001). *Probabilistic Model Code*, Joint Committee on Structural Safety (JCSS), Technical University of Denmark, Kongens Lyngby, Denmark, http://www.jcss.byg.dtu.dk/Publications/Probabilistic_Model_Code.

Kamranzad, B, Etemad-Shahidi, A, and Chegini, V (2013). "Assessment of Wave Energy Variation in the Persian Gulf," *Ocean Eng*, 70, 72–80. http://dx.doi.org/10.1016/j.oceaneng.2013.05.027.

Kriezi, EE, and Broman, B (2008). "Past and Future Wave Climate in the Baltic Sea Produced by the SWAN Model with Forcing from the Regional Climate Model RCA of the Rossby Centre," *US/EU-Baltic Int Symp*, Tallinn, Estonia, IEEE/OES, 1–7. http://dx.doi.org/10.1109/BALTIC.2008.4625539.

Lemaire, M, Chateauneuf, A, and Mitteau, JC (2009). *Structural Reliability*, ISTE, London, UK, 504 pp.

Liberti, L, Carillo, A, and Sannino, G (2013). "Wave Energy Resource Assessment in the Mediterranean: The Italian Perspective," *Renewable Energy*, 50, 938–949. http://dx.doi.org/10.1016/j.renene.2012.08.023.

Madsen, HO, Krenk, S, and Lind, NC (1986). *Methods of Structural Safety*, Prentice-Hall, Englewood Cliffs, NJ, USA, 403 pp.

Mazarakis, N, Kotroni, V, Lagouvardos, K, and Bertotti, L (2012). "High-Resolution Wave Model Validation over the Greek Maritime Areas," *Nat Hazards Earth Syst Sci*, 12, 3433–3440. http://dx.doi.org/10.5194/nhess-12-3433-2012.

MET (2011). *A High Resolution SWAN Model Assessment: North Norfolk to Humber*, Forecasting Research Technical Report 557, MET Office, Devon, UK.

Musić, S, and Nicković, S (2008). "44-Year Wave Hindcast for the Eastern Mediterranean," *Coastal Eng*, 55(11), 872–880. http://dx.doi.org/10.1016/j.coastaleng.2008.02.024.

Myrhaug, D, and Kjeldsen, SP (1986). "Steepness and Asymmetry of Extreme Waves and the Highest Waves in Deep Water," *Ocean Eng*, 13(6), 549–568. http://dx.doi.org/10.1016/0029-8018(86)90039-9.

Neill, SP, and Hashemi, MR (2013). "Wave Power Variability over the Northwest European Shelf Seas," *Appl Energy*, 106, 31–46. http://dx.doi.org/10.1016/j.apenergy.2013.01.026.

Pilar, P, Guedes Soares, C, and Carretero, JC (2008). "44-Year Wave Hindcast for the North East Atlantic European Coast," *Coastal Eng*, 55(11), 861–871. http://dx.doi.org/10.1016/j.coastaleng.2008.02.027.

Ponce de León, S, and Guedes Soares, G (2010). "The Sheltering Effect of the Balearic Islands in the Hindcast Wave Field," *Ocean Eng*, 37(7), 603–610. http://dx.doi.org/10.1016/j.oceaneng.2010.01.011.

Ponce de León, S, Bettencourt, JH, and Kjerstad, N (2011). "Simulation of Irregular Waves in an Offshore Wind Farm with a Spectral Wave Model," *Cont Shelf Res*, 31(15), 1541–1557. http://dx.doi.org/10.1016/j.csr.2011.07.003.

Ratsimandresey, AW, Sotillo, MG, Carretero Albiach, JC, Álvarez Fanjul, E, and Hajji, H (2008). "A 44-Year High-Resolution Ocean and Atmospheric Hindcast for the Mediterranean Basin Developed Within the HIPOCAS Project," *Coastal Eng*, 55(11), 827–842. http://dx.doi.org/10.1016/j.coastaleng.2008.02.025.

RCP GmbH (2004). *Comrel & Sysrel: User Manuals*, Reliability Consulting Programs GmbH, Munich, Germany.

Rusu, E, and Guedes Soares, C (2012). "Wave Energy Pattern Around the Madeira Islands," *Energy*, 45(1), 771–785. http://dx.doi.org/10.1016/j.energy.2012.07.013.

Rusu, E, Gonçalves, M, and Guedes Soares, C (2011). "Evaluation of the Wave Transformation in an Open Bay with Two Spectral Models," *Ocean Eng*, 38(16), 1763–1781. http://dx.doi.org/10.1016/j.oceaneng.2011.08.005.

Rusu, L, Pilar, P, and Guedes Soares, C (2008a). "Hindcast of the Wave Conditions along the West Iberian Coast," *Coastal Eng*, 55(11), 906–919. http://dx.doi.org/10.1016/j.coastaleng.2008.02.029.

Rusu, E, Pilar, P, and Guedes Soares, C (2008b). "Evaluation of the Wave Conditions in Madeira Archipelago with Spectral Models," *Ocean Eng*, 35(13), 1357–1371. http://dx.doi.org/10.1016/j.oceaneng.2008.05.007.

Sabique, L, Annapurnaiah, K, Balakrishnan Nair, TM, and Srinivas, K (2012). "Contribution of Southern Indian Ocean Swells on the Wave Heights in the Northern Indian Ocean: A Modeling Study," *Ocean Eng*, 43, 113–120. http://dx.doi.org/10.1016/j.oceaneng.2011.12.024.

Stopa, JE, et al. (2013). "Wave Energy Resources Along the Hawaiian Island Chain," *Renewable Energy*, 55, 305–321. http://dx.doi.org/10.1016/j.renene.2012.12.030.

SWAN Team (2013). *SWAN User Manual: SWAN Cycle III, version 40.91AB*, TU Delft, The Netherlands, http://www.swan.tudelft.nl/.

Tarp-Johansen, NJ, Sørensen, JD, and Madsen, PH (2002). "Experience with Acceptance Criteria for Offshore Wind Turbines in Extreme Loading," *Proc JCSS Workshop Reliability-Based Code Calibration*, Zurich, Switzerland, CD-ROM, http://www.jcss.ethz.ch/.

Tolman, HL (2009). *User Manual and System Documentation of WAVEWATCH III, version 3.14*, NOAA/NWS/NCEP/MMAB Technical Note 276.

WAMDI Group (Hasselmann, S, et al.) (1988). "The WAM Model: A Third-Generation Ocean Wave Prediction Model," *J Phys Oceanogr*, 18, 1775–1810. http://dx.doi.org/10.1175/1520-0485(1988)018%3C1775:TWMTGO%3E2.0.CO;2.

Zheng, C, Pan, J, and Li, J (2013). "Assessing the China Sea Wind Energy and Wave Energy Resources from 1988 to 2009," *Ocean Eng*, 65, 39–48. http://dx.doi.org/10.1016/j.oceaneng.2013.03.006.

APPENDIX

The collected validation data from published articles is shown in Table 7.

Wave model	Reference	Wave model	Reference
MIKE21 SW	DHI (2013b)	SWAN	Neill and Hashemi (2013)
MIKE21 SW	Sabique et al. (2012)	MIKE21 SW	Aydoğan et al. (2013)
SWAN	Akpınar et al. (2012)	SWAN	Stopa et al. (2013)
SWAN	Rusu et al. (2008a)	WAM	Carretero Albiach et al. (2000)
WAM	Ponce de León et al. (2011)	WAM	Ratsimandresey et al. (2008)
WAM	Cieślikiewicz and Paplińska-Swerpel (2008)	WW III	Chawla et al. (2013)
WAM	Musić and Nicković (2008)	SWAN	MET (2011)
SWAN	Rusu and Guedes Soares (2012)	WAM	Dykes et al. (2002)
WAM	Ponce de León and Guedes Soares (2010)	SWAN	Dykes et al. (2002)
MIKE21 SW	Ayat (2013)	WAM	Berg (2008)
WAM	Pilar et al. (2008)	MIKE21 SW	Holbom (2011)
WW III	Zheng et al. (2013)	WAM	Mazarakis et al. (2012)
SWAN	Rusu et al. (2008b)	WAM	Gorman et al. (2003)
SWAN	Bolaños-Sanchez et al. (2007)	SWAN	Kriezi and Broman (2008)
WAM	Bolaños-Sanchez et al. (2007)	SWAN	Bento et al. (2011)
WAM	Liberti et al. (2013)	SWAN	Kamranzad et al. (2013)
SWAN	Rusu et al. (2011)		

Table 7 Information about the considered validation data for different wave models and published articles